Available online at www.sciencedirect.com
ScienceDirect
Computers & Fluids 35 (2006) 1137–1153
computers & fluids
www.elsevier.com/locate/compfluid

Lattice BGK direct numerical simulation of fully developed turbulence in incompressible plane channel flow

P. Lammers, K.N. Beronov *, R. Volkert, G. Brenner, F. Durst

Institute of Fluid Mechanics, Friedrich–Alexander University Erlangen—Nuremberg, Cauerstrasse 4, D-91058 Erlangen, Germany

Received 6 September 2002; received in revised form 10 August 2005; accepted 10 October 2005
Available online 26 January 2006

Abstract

Over the last decade, lattice Boltzmann methods have proven to be reliable and efficient tools for the numerical simulation of complex flows. The specifics of such methods as turbulence solvers, however, are not yet completely documented. This paper provides results of direct numerical simulations (DNS), by a lattice Boltzmann scheme, of fully developed, incompressible, pressure-driven turbulence between two parallel plates. These are validated against results from simulations using a standard Chebyshev pseudo-spectral method. Detailed comparisons, in terms of classical one-point turbulence statistics at moderate Reynolds number, with both numerical and experimental data show remarkable agreement.

Consequently, the choice of numerical method has, in sufficiently resolved DNS computations, no dominant effect at least on simple statistical quantities such as mean flow and Reynolds stresses. Since only the method-independent statistics can be credible, the choice of numerical method for DNS should be determined mainly through considerations of computational efficiency. The expected practical advantages of the lattice Boltzmann method, for instance against pseudo-spectral methods, are found to be significant even for the simple geometry and the moderate Reynolds number considered here. This permits the conclusion that the lattice Boltzmann approach is a promising DNS tool for incompressible turbulence.

1. Introduction

Computational fluid dynamics (CFD) has grown out of 50 years of continuous development and improvement of computational hardware and of numerical algorithms for solving various kinds of partial differential equations. Over the last several decades, CFD has become a popular tool for flow engineering and for fundamental research in fluid mechanics. However, some problems of great complexity remain open, despite the enormous effort invested. One of them is the description of turbulence with sufficient details to yield information that permits deeper insights into the nature of turbulence. Over the last 20 years, direct numerical simulations (DNS) have been applied to investigate a large number of canonical turbulent flows and have provided new and deeper insights into the mechanisms and the details of turbulent mixing and turbulent transport of mass, momentum, and energy. The data gained from adequately conducted DNS can be more reliable and informative than results obtained by alternative methods, e.g., experimental or analytical. DNS predictions, however, still remain confined to relatively low Reynolds number flows, essentially owing to computing hardware limitations.

For flows in simple geometries, algorithms based on spectral methods for spatial discretization have been most successful in numerically solving the Navier–Stokes equation, due to their excellent precision while providing flow computations at reasonable cost. Attempts have been made to simulate turbulence using finite-difference, finite-volume, and finite-element spatial discretizations. The numerical solutions resulting from such attempts have been shown to be, as expected, of lower quality than pseudo-spectral ones, when compared at fixed temporal and spatial

* Corresponding author. Tel.: +49 9131 852 8280; fax: +49 9131 582 9503.
E-mail address: kberonov@lstm.uni-erlangen.de (K.N. Beronov).

0045-7930/$ - see front matter © 2005 Elsevier Ltd. All rights reserved.
doi:10.1016/j.compfluid.2005.10.002

resolutions. On the other hand, they have allowed relatively efficient flow simulations in complex flow domain geometries. Extensions of pseudo-spectral methods to such geometries, e.g., by spectral element approaches, have proven to be cumbersome. It remains an open problem to identify a numerical method which presents the best compromise between the two conflicting requirements for turbulence simulations: (i) low complexity and computational cost for complex problems and (ii) high quality of the numerical simulation results.

The present authors advocate, on the basis of their own investigations, lattice Boltzmann algorithms as the best candidates for such an optimal approach towards numerical simulations of incompressible turbulence. It is already well known that lattice Boltzmann methods are robust and easy to use in complex flow geometries, but experience has been accumulated mostly with low-Reynolds-number flows. The present paper aims to demonstrate that these methods are also well suited for predicting fully developed turbulence through direct numerical simulation. Previous applications of lattice Boltzmann codes to turbulence have mostly been focused on developed channel flows [1,9,25]. Recent investigations by the present authors show, however, that those previous simulations lacked the spatial extent (especially in the mean flow direction) required to capture correctly the features of developed wall-bounded turbulence in channel flows.

The simulations described here are concerned, like the previous studies cited above, with developed channel turbulence. Studying plane channel flow allows a detailed verification of the lattice Boltzmann predictions through comparison with numerous available databases, including the standard DNS of channel turbulence documented in [18] and in other related papers. Although some previous lattice Boltzmann simulations [25] have addressed complex issues such as the structure functions of the fluctuating velocity components, only the simplest turbulence statistics will be considered here. This necessary first step must be carried out carefully, as it can, and indeed does, lead to important and unexpected findings. Technically, the application of lattice Boltzmann methods to turbulence DNS can be readily extended to problems with, say, flow separation or laminar-to-turbulent transition. The channel flow data presented here strongly suggest that encouraging results can be expected in carrying out predictions of these turbulent flows.

The lattice Boltzmann methodology and the particular lattice Boltzmann method used are presented in detail in Section 2. The material is in most parts not new, but is put together for the general reader's convenience. In Section 3, the relevant physical and computational aspects of developed channel flow turbulence simulation are introduced. Implementation and performance details of the lattice Boltzmann code employed are provided in Section 4, including a comparison with the performance of a standard pseudo-spectral code. Results for turbulence statistics obtained with the help of the new lattice Boltzmann code are presented in Section 5 and compared against the same statistics obtained by other methods. Conclusions and comments based on the presented results are given in Section 6.

2. The lattice Boltzmann model

Computationally, the lattice Boltzmann methods are based on discretizations of kinetic equations for one-point distribution functions $f(t,\boldsymbol{x},\boldsymbol{\xi})$ arising in statistical kinetic theories, such as that of rarefied gases. The earliest and most important instance of such an equation is the Boltzmann equation, the backbone of the gas-kinetic theory. Such kinetic equations can be put in the general form

$$\partial_t f + \boldsymbol{\xi}\cdot\nabla_{\boldsymbol{x}} f + \boldsymbol{g}\cdot\nabla_{\boldsymbol{\xi}} f = \Omega[f,\bar{f}], \tag{1}$$

where $\bar{f}$ is the equilibrium distribution function, $\boldsymbol{\xi}$ is a virtual velocity vector independent of time t and location $\boldsymbol{x}$, all external forces are lumped into $\boldsymbol{g}$, and the intrinsic physics of the system is reflected by the collision term Ω. The Navier–Stokes equations can be derived from such kinetic equations, with appropriate assumptions about Ω and about a scale separation between the relevant dynamic scales of the kinetic equation (short) and the macroscopic hydrodynamic scales (long). The fluid density, velocity, and stresses (including pressure) are then computed as the lowest-order moments of the distribution function f with respect to integration over $\boldsymbol{\xi}$-space, which has the same dimension d as the $\boldsymbol{x}$-space of Euclidean coordinates.

The discretization of that space in lattice Boltzmann methods follows by employing a discrete velocity model for the kinetic equation, that is, by replacing $f(t,\boldsymbol{x},\boldsymbol{\xi})$ by a finite-dimensional vector $\boldsymbol{f}(t,\boldsymbol{x}) = (f_{-m},\ldots,f_{-1},f_0, f_1,\ldots,f_m)$, approximating the $\boldsymbol{\xi}$-moments through corresponding quadratures, so that, in particular, the density and velocity of the fluid are defined as

$$\rho(t,\boldsymbol{x}) = \sum_{j=-m}^{m} f_j(t,\boldsymbol{x}), \quad \rho(t,\boldsymbol{x})\boldsymbol{v}(t,\boldsymbol{x}) = \sum_{j=-m}^{m} f_j(t,\boldsymbol{x})\boldsymbol{\xi}_j, \tag{2}$$

and then solving the system ($-m \leqslant j \leqslant m$) of PDEs

$$\partial_t f_j + \boldsymbol{\xi}_j\cdot\nabla_{\boldsymbol{x}} f_j = \Omega_j[\boldsymbol{f},\bar{\boldsymbol{f}}] + F_j[\boldsymbol{g},\bar{\boldsymbol{f}}], \tag{3}$$

where f_j is the distribution function (in the virtual velocity space) corresponding to $\boldsymbol{\xi}_j$. An expression F_j, particular to each discrete velocity model, is used to model the term $\boldsymbol{f}\cdot\nabla_{\boldsymbol{\xi}} f$. In our case, $\boldsymbol{g}$ is the external forcing prescribed in the corresponding Navier–Stokes equation.

Specification of the kinetic theory underlying a discrete velocity model includes a pressure definition (e.g., by a simplified equation of state $E(p,\rho) = 0$, or as a second moment of f in $\boldsymbol{\xi}$) and an explicit form for the collision term Ω.

2.1. The BGK model

A simple choice of Ω in (1) for the purpose of predicting fluid flow dynamics is the linear, single-relaxation-time model, introduced by Bhatnagar et al. [3]:

$$\Omega[f,\bar{f}] = \big(\bar{f}(\rho,\boldsymbol{v}) - f(t,\boldsymbol{x},\boldsymbol{\xi})\big)\omega, \tag{4}$$

$$\bar{f} = \left(2\pi c_s^2\right)^{-d/2}\rho\exp\left(-\|\boldsymbol{\xi}-\boldsymbol{v}\|^2/2c_s^2\right). \tag{5}$$

The scalar $1/\omega$ is the single-relaxation-time parameter of the model and is related to the Newtonian viscosity of the Navier–Stokes equation that can be obtained analytically from the BGK model. The equilibrium distribution function $\bar{f}$ prescribed in (5) has the "shifted Maxwellian" form well known from the classical gas-kinetic theory. The replacement of the usual term $k\theta$ in (5), where k is the Boltzmann constant and θ is the absolute temperature, by

$$p/\rho = c_s^2 = \text{constant}. \tag{6}$$

is specific to the lattice Boltzmann context. The notion of a "speed of sound" c_s is borrowed from ideal gas dynamics, but fixing it to a constant is an additional, technical aspect of lattice Boltzmann theory, essential in deriving the Navier–Stokes dynamics from the kinetic equation for f.

This BGK model for the relaxation mechanism assures that all distribution functions f tend to remain close to their equilibrium values $\bar{f}$. Such proximity is a precondition for the validity of the Chapman–Enskog expansion, the procedure which defines the relationship between the lattice Boltzmann and the Navier–Stokes dynamics. That procedure is a singular asymptotic series expansion whose small parameter effectively represents the smallness of deviations from kinetic theory equilibrium. Formally, the small parameter is introduced into the theory as a scale separation measure, valid for both time and length scales: it is assumed that the smallest characteristic scales of the hydrodynamics are much larger than the characteristic scales of the kinetics described directly by (1).

In addition to the BGK scheme, there exist, of course, other linear relaxation schemes for Ω. Like the BGK collision operator, they act to reduce the difference between the instantaneous densities f_j and their equilibrium counterparts $\bar{f}_j$, but not in a uniform way: different $\boldsymbol{\xi}$-moments are damped at different rates, explaining the name multiple-relaxation-time (MRT) lattice Boltzmann schemes. Such schemes, alternatively called moment-relaxation models, have advantages concerning the stability of numerical simulation [7]. Their advantages have been demonstrated in a number of applications, including one large-eddy simulation of turbulence LES [20]. In the present study, the standard BGK lattice Boltzmann scheme was used for its simplicity.

2.2. Lattice model

The choice of a particular lattice model includes the prescription of (i) a set of discrete velocity model vectors $\{\boldsymbol{\xi}_j\}$ that discretizes the virtual velocity space and (ii) a corresponding equilibrium distribution $\bar{f}_j$ of distribution functions for the discrete velocities. The three-dimensional lattice model used here is the 19-velocity D3Q19 model [24], obtained as a projection from 4D on to 3D space of the face-centered hypercubic (FCHC) lattice [2], which guarantees sufficient symmetry to reproduce the Navier–Stokes equation on a Chapman–Enskog expansion. The discrete velocities of the D3Q19 model can be enumerated in many ways; one that emphasizes the symmetry of the lattice is the following:

$$\begin{aligned}
&\boldsymbol{\xi}_0 = (0,0,0),\\
&\boldsymbol{\xi}_1 = (+,0,0), \quad \boldsymbol{\xi}_2 = (+,+,0), \quad \boldsymbol{\xi}_3 = (0,+,0),\\
&\boldsymbol{\xi}_{-1} = (-,0,0), \quad \boldsymbol{\xi}_{-2} = (-,-,0), \quad \boldsymbol{\xi}_{-3} = (0,-,0),\\
&\boldsymbol{\xi}_4 = (0,+,+), \quad \boldsymbol{\xi}_5 = (+,0,+), \quad \boldsymbol{\xi}_6 = (+,+,0),\\
&\boldsymbol{\xi}_{-4} = (0,-,-), \quad \boldsymbol{\xi}_{-5} = (-,0,-), \quad \boldsymbol{\xi}_{-6} = (-,-,0),\\
&\boldsymbol{\xi}_7 = (0,+,-), \quad \boldsymbol{\xi}_8 = (-,0,+), \quad \boldsymbol{\xi}_9 = (+,-,0),\\
&\boldsymbol{\xi}_{-7} = (0,-,+), \quad \boldsymbol{\xi}_{-8} = (+,0,-), \quad \boldsymbol{\xi}_{-9} = (-,+,0),
\end{aligned} \tag{7}$$

where $(+,0,-)$ stands, for example, for the vector $(\Delta x, 0, -\Delta z)$ with

$$\Delta x = \Delta y = \Delta z = \Delta,$$

on a regular Cartesian grid, at whose nodes $\boldsymbol{x} = (x,y,z) = (j_x\Delta, j_y\Delta, j_z\Delta)$ with integer j_x, j_y, j_z, the discrete analogs of all dynamic fields, such as f_α and $\boldsymbol{v}$, are given.

The relation between the relaxation time $1/\omega$ of the BGK model at the level of the one-point statistical description of "microscopic" dynamics and the kinematic viscosity of the corresponding Navier–Stokes equation at the macroscopic level is

$$\nu = c_s^2/\omega,$$

obtained as part of the result of a Chapman–Enskog expansion [13].

In order to prescribe an equilibrium which is readily computable and analytically tractable in the discrete model context, it is customary to assume the validity of a "low-Mach-number" approximation,

$$Ma = v/c_s \ll 1, \quad v(t,\boldsymbol{x}) = \|\boldsymbol{v}\|, \tag{8}$$

i.e., that the Navier–Stokes dynamics evolves at low velocity and thus over long times, when measured in lattice units. Although formally independent, this requirement appears to be in qualitative agreement with a previously mentioned prerequisite for the Chapman–Enskog analysis, namely that deviations from equilibrium are small.

In the low-Mach-number approximation, the Maxwellian equilibrium distribution can be discretized and approximated up to second order in Ma, yielding a computationally convenient prescription of the equilibrium distribution functions $\bar{f}_\alpha$:

$$\begin{aligned}
&\bar{f}_\alpha(t,\boldsymbol{x}) = \mathrm{w}(\|\boldsymbol{\xi}_\alpha\|^2)\rho\left(1 + 3v_\alpha + \tfrac{9}{2}v_\alpha^2 - \tfrac{3}{2}|\boldsymbol{v}|^2\right),\\
&v_\alpha = \boldsymbol{v}(t,\boldsymbol{x})\cdot\boldsymbol{\xi}_\alpha.
\end{aligned} \tag{9}$$

The weight coefficients must be chosen to give

$$\sum_\alpha \bar{f}_\alpha = \rho, \quad \sum_\alpha \bar{f}_\alpha \boldsymbol{\xi}_\alpha = \rho \boldsymbol{v}, \\ \sum_\alpha \bar{f}_\alpha \boldsymbol{\xi}_\alpha \boldsymbol{\xi}_\alpha = \rho(\boldsymbol{v}\boldsymbol{v} + c_s^2 \boldsymbol{I}). \tag{10}$$

They have been shown [14] to correspond to a Gaussian quadrature of the minimal order required to reproduce correctly the spatial symmetries of the Navier–Stokes equation.

The D3Q19 discrete model used here, with already fixed form of the equilibrium function and of the (BGK or multiple-relaxation-time) collision operator Ω, then completely specified if the value of c_s and of the quadrature weights in $\bar{f}_\alpha$ are given. It is readily seen that the symmetries of the system (7) of discrete vectors imply $\sum_\alpha \boldsymbol{\xi}_\alpha \boldsymbol{\xi}_\alpha = \boldsymbol{I}/3$ and $\sum_\alpha \boldsymbol{\xi}_\alpha = 0$, and that with (10) these lead to the unique choice

$$c_s = \tfrac{1}{\sqrt{3}}, \quad \mathrm{w}(0) = \tfrac{1}{3}, \quad \mathrm{w}(1) = \tfrac{1}{18}, \quad \mathrm{w}(2) = \tfrac{1}{36}. \tag{11}$$

2.3. Time discretization and forcing

The lattice Boltzmann method is obtained by a finite-difference discretization of the discrete velocity model equation:

$$f_\alpha(t + \Delta t, \boldsymbol{x} + \boldsymbol{\xi}_\alpha) = f_\alpha(t, \boldsymbol{x}) - \omega \Delta t \big(f_\alpha(t, \boldsymbol{x}) - \bar{f}_\alpha(t, \boldsymbol{x})\big). \tag{12}$$

This is a characteristic finite-difference method for the numerical integration of the lattice BGK equation. It is formally of first order in Δt.

By modifying the relaxation parameter, however,

$$\frac{1}{\omega} = \frac{3}{\nu} + \frac{1}{2}, \tag{13}$$

it is made second-order precise as far as the time step Δt and the effective Navier–Stokes dynamics, simulated by the lattice BGK scheme over the "slow scales" implicit in the Chapman–Enskog analysis, are concerned. Leading orders of terms neglected in the course of the Chapman–Enskog analysis [12] are $\mathrm{O}(|\boldsymbol{v}|^3)$, and $\mathrm{O}(\nabla_{\boldsymbol{x}} \cdot \boldsymbol{v})$.

The channel flow to be treated here is driven by a constant pressure gradient:

$$\boldsymbol{f} = -\nabla_{\boldsymbol{x}} p.$$

This forcing term can be included in an augmented form of (12) by any of the methods described in the literature, most of which modify either the post-collision velocities or the right-hand side of the kinetic equation, or both. For a list of such options and basic references, see [4,11]. The simplest way to modify the velocity (used also in production codes, see, e.g., [27]) is

$$\Omega_\alpha[\boldsymbol{f}, \bar{\boldsymbol{f}}] + F_\alpha[\boldsymbol{g}, \bar{\boldsymbol{f}}] = \Omega_\alpha[\boldsymbol{f}, \bar{\boldsymbol{f}}^*], \\ \bar{\boldsymbol{f}}^*[\rho, \boldsymbol{v}] = \bar{\boldsymbol{f}}[\rho, \boldsymbol{v} + \boldsymbol{f}/\rho]. \tag{14}$$

To retain second-order accuracy, one takes

$$\Omega_\alpha[\boldsymbol{f}, \bar{\boldsymbol{f}}] + F_\alpha[\boldsymbol{g}, \bar{\boldsymbol{f}}] = \tfrac{1}{2}(\Omega_\alpha[\boldsymbol{f}, \bar{\boldsymbol{f}}] + \Omega_\alpha[\boldsymbol{f}, \bar{\boldsymbol{f}}^*]), \tag{15}$$

$$\rho(t, \boldsymbol{x}) \boldsymbol{v}(t, \boldsymbol{x}) = \left(\sum_\alpha f_\alpha(t, \boldsymbol{x}) \boldsymbol{\xi}_\alpha\right) + \frac{\Delta t}{2} \boldsymbol{f}(t, \boldsymbol{x}). \tag{16}$$

The result (16) can be obtained also if, instead of (15), one takes $\Omega_\alpha + F_\alpha$ with

$$F_\alpha[\boldsymbol{g}, \bar{\boldsymbol{f}}] = \frac{\Delta t}{2} \bar{f}_\alpha \boldsymbol{\xi}_\alpha \cdot \boldsymbol{f}. \tag{17}$$

2.4. Incompressible flow DNS

A modification to lattice Boltzmann schemes of the kind described above has been proposed [12] for low-Reynolds-number incompressible flows. While the standard schemes advance directly the local fluid density ρ and momentum $\rho \boldsymbol{v}$, their "incompressible" counterparts assume that the density distribution represents small perturbations about a constant $\rho_0 = \mathrm{O}(1)$, i.e., that $\rho = \rho_0 + \delta\rho$ where $\delta\rho = \mathrm{O}(Ma^2) \ll 1$. This suggests redefining

$$f_\alpha^{\mathrm{new}} \leftarrow c_s^2 f_\alpha, \quad \bar{f}_\alpha^{\mathrm{new}} \leftarrow c_s^2 \bar{f}_\alpha,$$

and expanding systematically in orders of Ma. Neglecting $\mathrm{O}(Ma^3)$ terms and omitting the superscript $(\cdot)^{\mathrm{new}}$, one obtains the "incompressible" model D3Q19i:

$$\bar{f}_\alpha(t, \boldsymbol{x}) = \mathrm{w}(|\boldsymbol{\xi}_\alpha|^2) p_0 \left(\frac{p}{p_0} + 3 v_\alpha + \frac{9}{2} v_\alpha^2 - \frac{3}{2} |\boldsymbol{v}|^2\right), \tag{18}$$

$$p(t, \boldsymbol{x}) = \sum_{\alpha=-9}^{9} f_\alpha(t, \boldsymbol{x}), \quad \boldsymbol{v}(t, \boldsymbol{x}) = \frac{1}{p_0} \sum_{\alpha=-9}^{9} f_\alpha(t, \boldsymbol{x}) \boldsymbol{\xi}_\alpha, \tag{19}$$

$$(\partial_t + \boldsymbol{v} \cdot \nabla_{\boldsymbol{x}}) \boldsymbol{v} = \nabla_{\boldsymbol{x}} \cdot \nu \Big(\nabla_{\boldsymbol{x}} \boldsymbol{v} + (\nabla_{\boldsymbol{x}} \boldsymbol{v})^{\mathrm{T}}\Big) - \nabla_{\boldsymbol{x}} p, \tag{20}$$

$$\partial_t p = -(\nabla_{\boldsymbol{x}} \cdot \boldsymbol{v}) c_s^2. \tag{21}$$

Up to the neglected terms, this scheme will obviously enforce incompressibility on steady solutions, in view of (21), but not necessarily on transient solutions. The "incompressible" lattice Boltzmann methods of this kind bear a resemblance to the artificial compressibility schemes used in some incompressible Navier–Stokes solvers. The macroscopic equations obtained by the Chapman–Enskog analysis [12] include the usual Navier–Stokes momentum equation along with (19), which replaces the strict solenoidality condition $(\nabla_{\boldsymbol{x}} \cdot \boldsymbol{v}) = 0$. Even for unsteady solutions that are resolved in time by the discrete algorithm, it will imply $\nabla_{\boldsymbol{x}} \cdot \boldsymbol{v} \leqslant \mathrm{O}(Ma^2)$. Expecting $|\nabla_{\boldsymbol{x}} \cdot \boldsymbol{v}| \ll \|\boldsymbol{v}\|$, it is clear that the right–hand side of (21) introduces less error than its counterpart in the original lattice model, which is

$$\partial_t \rho = -(\nabla_{\boldsymbol{x}} \cdot \boldsymbol{v}) - \boldsymbol{v} \cdot \nabla_{\boldsymbol{x}} \rho,$$

instead of $\rho = 1$. In practice, the use of "incompressible" lattice schemes reduces significantly the intensity of numerical "pressure waves" and improves the precision of transient simulations with respect to incompressibility and predicted pressure.

2.5. Initial and boundary conditions

The initial velocity fields in the present simulations are constructed as discretization of analytic fields that satisfy incompressibility exactly and are negligibly small at the solid walls. A particular specification assuring sustained turbulence at long times is given in Section 3.2.

The velocity data are then transformed into distribution functions, using the equilibrium distribution (9). That is, at the initial time $t = 0$ it is set

$$f_\alpha(0, \boldsymbol{x}) = \bar{f}_\alpha[\rho, \boldsymbol{v}(0, \boldsymbol{x})], \quad \rho(0, \boldsymbol{x}) = \rho_0 = 1. \tag{22}$$

It is more consistent to initialize also the nonequilibrium parts of the PDFs, using the analytically computable stress field of the initial velocity. This would also save computing time otherwise needed to relax these nonequilibrium parts to a state consistent with the macroscopic stress. In practice, however, these issues are of small importance. For example, the number of iterations required for the relaxation of the nonequilibrium parts of PDFs depends only weakly on the resolution and is considerably shorter than the time of the transient from the initial flow field to developed turbulence.

Considering the non-slip condition at solid–fluid boundaries, the simplest way to impose exact mass conservation (no penetration, zero normal flux) and approximate non-slip (small tangential flux) is to apply

$$f_\alpha(t + \Delta t, \boldsymbol{x}) = f_{-\alpha}(t, \boldsymbol{x}) \tag{23}$$

at each time step and at each lattice node in the flow domain, whose immediate neighbor along the $\boldsymbol{\xi}_\alpha$ direction is within the solid. This so-called "bounce-back" condition is the most commonly used one at solid walls, because of its simplicity, robustness and exact mass conservation. In general, it is a first-order approximation, which can influence the overall precision of the simulation. For the special case of walls aligned with some of the lattice stencil directions, however, it can be shown to be of second order, as done for a two-dimensional case in [15]. In that case, the solid boundary is effectively placed half-way between two neighboring nodes. This is referred to in the literature as bounce-back on the link (BBL). It has been shown mathematically that BBL is in general of first order, but is of second order in parallel channels aligned with the grid. For the simple flow considered in the present paper, such an alignment is imposed in a natural way. The reported simulations are therefore of second order in the (small) ratio of Δt to some characteristic hydrodynamic time scale, such as t_c defined in Section 3.1 (in the presented simulations, $\Delta t/t_c = \mathrm{O}(10^{-4})$), also in view of the coupling between spatial and time step size.

3. The set-up of plane channel turbulence DNS using a lattice Boltzmann method

Plane channel flow turbulence is particularly well studied and abundant data from simulations and from laboratory measurements are available. Particularly well known is a Chebyshev pseudo-spectral direct numerical simulation [18] at $Re_\tau = 180$. This is a moderate but definitely turbulent value for Re_τ, a Reynolds number used in turbulence modeling of channel flows and defined later in (24). Turbulence statistics from that simulation are part of a publicly available standard DNS database on plane channel turbulence [21].

The features of the lattice Boltzmann code and its performance are discussed in Section 4. A comparison of the turbulence predictions obtained with the code with those found in the above-mentioned database is given in Section 5. Before that, the physical and numerical set-up of the lattice Boltzmann DNS are presented.

3.1. The physical problem

The flow between two parallel flat walls, with periodic boundary conditions for the velocity along the two spatial directions parallel to these walls, is referred to as (plane) Poiseuille flow or two-dimensional channel flow.[1] In a standard setting, this flow is driven either by a constant body force (uniform pressure drop) or by a prescribed flow rate. The laminar flow regime is stable at sufficiently low Reynolds numbers Re and is of no interest here. At sufficiently high Re the flow is always turbulent. Features of transition to turbulence (intermittency, essential dependence on flow history and on details of forcing and perturbation) are relevant only over an intermediate range of Reynolds numbers.

Fully developed turbulence can be experimentally observed in sufficiently long channels, far from the inlet, the outlet, and from any symmetry-breaking geometry features such as side walls. In the canonical setting considered here, periodic boundary conditions are imposed in the streamwise direction, corresponding to the x-coordinate in this paper, and in the spanwise direction, along the z-coordinate. In the direction normal to the wall, along the y-coordinate, non-slip conditions are imposed at the parallel walls, which are assumed to be located at $y = \pm H$. Obviously, H stands for the channel half-width. In this canonical setting, the regime of fully developed turbulence can be observed for a sufficiently long time after flow onset and corresponds to the so-called statistically steady state, in which the turbulence statistics are time-independent. All results in Section 5 pertain to this regime.

The dynamic fields of interest are the components ($i = x, y, z$) of the turbulent velocity $\boldsymbol{v} = (v_x, v_y, v_z)$, and the

[1] The latter name indicates that this is a plane-parallel flow, i.e., having only one direction of velocity in the laminar regime, and of mean velocity in the turbulent regime, which is constant and orthogonal to the direction of the gradient of that velocity. Hence, only two directions are essential in describing the flow—that normal to the wall (y-coordinate) and that along the (mean) flow direction (x-coordinate). Of course, the instantaneous full velocity field is three-dimensional in the turbulent regime, but its one-point statistics depend, like the mean profile, only on y.

pressure p. The corresponding mean fields are $U = \langle v_x \rangle$ and $P = \langle p \rangle + Gx$, where $-G$ is the constant pressure gradient driving the flow,

$$0 = G + \nu(\mathrm{d}/\mathrm{d}y)^2 U(y),$$

and ν is the kinematic viscosity. The turbulent fluctuations are $v_x' = v_x - U$, $v_y' = v_y$, $v_z' = v_z$, and $p' = p - P + G$. Only one-point, low-order moments of these fluctuations will be considered in the data comparison that follows in Section 5: second-order moments are quantified by the Reynolds stresses

$$R_{ij} = R_{ji} = \left\langle v_i' v_j' \right\rangle, \quad i,j = x,y,z,$$

whereby $R_{xz} = R_{xz} = 0$, and by the pressure autocorrelation $\langle (p')^2 \rangle$. Third-and fourth-order moments are quantified by skewness and flatness factors of individual velocity components:

$$S_j = S[v_j'] = \left\langle (v_j')^3 \right\rangle \Big/ \left\langle (v_j')^2 \right\rangle^{3/2},$$

$$F_j = F[v_j'] = \left\langle (v_j')^4 \right\rangle \Big/ \left\langle (v_j')^2 \right\rangle^{2}.$$

In order to obtain converged statistics, the simulation is carried out is several steps: (i) an initial state, given as superposition of analytic and random components is selected and evolved to produce channel turbulence. (ii) This turbulence is evolved to a state that can be considered statistically steady as far as mean fields are concerned. (iii) Using the already converged mean fields, the required statistics of the fluctuating fields are accumulated. Considerably longer simulation times are required for convergence of two-point and higher-order one-point statistics than for those listed above.

With increasing Reynolds number, the structure of turbulence near the wall tends to an asymptotic state, whereby different layers of turbulence, located at different distances from the wall, approach this state at different times, depending on their separation from the wall. In fully turbulent channel flows away from the wall, a kind of self-similar turbulence cascade dominated by inertial effects can be discerned [22]. Most of the interesting physics, however, including the generation of turbulence [17], take place near the wall, where all forces involved—pressure, viscosity, and inertial forces—are of comparable importance. This region can be considered already close to its asymptotic state at the Reynolds number simulated in this study, whereas the inertia-dominated region cannot. The latter would contain a log-layer only at significantly higher Reynolds numbers.

To define a Reynolds number, it is first recalled that there are several customary units of lengths for the present canonical type of flow, including the channel width (or half-width H) and the "wall unit" or viscous length $\delta_\tau = \nu/u_\tau$. The skin friction velocity u_τ is defined through $u_\tau^2 = GH/\rho$. A density of $\rho = 1$ can be assumed throughout, since one is free to set the mass unit. Standard Reynolds number definitions are the centerline Reynolds number, $Re_c = HU_c/\nu$, where $U_c = U(0)$ is the centerline mean velocity, the bulk Reynolds number, $Re_m = 2HU_m/\nu$, where $U_m = \int_{-H}^{H} U(y)\,\mathrm{d}y/2H$ is the bulk-flow velocity, and the friction Reynolds number,

$$Re_\tau = Hu_\tau/\nu, \tag{24}$$

which implies $Re_\tau = H/\delta_\tau = H^+$. As usual, a superscript $(+)$ indicates quantities measured in the "wall units" δ_τ and u_τ. In a developed turbulent channel flow beyond the transient range of Reynolds numbers, $Re_m > Re_c \gg Re_\tau$. Hereafter, only Re_τ will be used. The corresponding "wall unit" of time is $t_\tau = \delta_\tau/u_\tau$. It will be useful further to introduce another time scale, $t_c \gg t_\tau$, quantifying the time taken by the very slow flow in the viscous sublayer to traverse distances comparable to the channel width:

$$t_c = t_\tau Re_\tau = H/u_\tau = \nu H^2/G. \tag{25}$$

3.2. Flow set-up

To carry out direct numerical simulation of plane channel turbulence, the non-dimensional physical parameters describing the problem must be defined first. Ideally, the Reynolds number alone should suffice, but in practice the spatial extent of the computational domain, $L_x{:}2H{:}L_z$, plays a significant role, so that the aspect ratios $\alpha_x = L_x/H$ and $\alpha_z = L_z/H$ must also be specified. In [18,21] the $Re_\tau = 180$ simulations were carried out for $\alpha_x = 4\pi$ and $\alpha_z = 4\pi/3 \approx 4.2$; the DNS results presented in Section 5 are for $\alpha_x = 16$ and $\alpha_z = 1$. Owing to the very long streamwise correlation lengths in wall-bounded turbulence, it is necessary to take large α_x. Indications and discussions of the existence of large streamwise flow structures can be found scattered in the literature, e.g., in [19] (experimental) and [16] (numerical, $\alpha_x \approx 25$). The aspect ratios selected here were determined after an extensive study of their effect on the considered one-point statistics. A detailed report of this study, including DNS runs at fixed Reynolds numbers and grid resolutions $\Delta^+ = \Delta/\delta_\tau$ but different aspect ratios, and of related studies on streamwise correlations will be given elsewhere.

Once Re_τ is prescribed, the choice of u_τ and of the grid step size Δ^+ (measured in wall units) follows from numerical resolution and stability considerations, cf. Section 3.4. Then the numerical values for the driving pressure gradient G and the BGK relaxation parameter ω, related to viscosity through (13), are not additional physical input data but must instead be determined from an "inversion" of the definitions of the wall units: $\nu = u_\tau \delta_\tau$ and $G = u_\tau^2/(\delta_\tau Re_\tau)$, where $H = \delta_\tau Re_\tau$ and $\rho = 1$ are recalled in writing the latter equation. It is further noted that $\delta_\tau = \Delta/\Delta^+$ and thus that $Re_\tau/\Delta^+ = H/\Delta = N_y/2$, where N_y is the number of grid steps between the opposite walls in a direction normal to the walls. With the bounce-back rule, this is also the distance between the walls when measured in the "lattice units" (in which the constant time step $\Delta t = 1$ and the lattice Boltzmann grid step $\Delta = 1$), while the num-

ber of grid points inside the flow domain is $N_y - 1$ along the y direction. Transforming everything to "lattice units," the rules for computing the required parameters become

$$\frac{2}{\omega} = 1 + \frac{6\Delta^+}{u_\tau} = 1 + \frac{3N_y}{u_\tau Re_\tau}, \quad G = u_\tau^2 \frac{\Delta^+}{Re_\tau} = \frac{2u_\tau^2}{N_y}. \tag{26}$$

The first rule agrees, of course, with the constraint $0 < \omega < 2$, imposed by the conditional stability of the explicit Euler scheme (12).

The initial field was based on a frequently used engineering approximation for the universal (high Re) mean velocity profile near the wall:

$$U^+(y^+) = \begin{cases} y^+ & \text{when } y^+ \leqslant y_w, \\ \ln(y^+)/\kappa + B & \text{when } y^+ > y_w, \end{cases}$$

where $\ln(y)$ denotes the natural logarithm of y. The particular values chosen, $y_w = 11.6$ for the U-profile inflection point, $\kappa = 0.4$ for the van Kármán constant, and $B = 5.2$, are not expected to have an impact on the eventual flow profile taken for the computation of developed turbulence statistics.

To obtain turbulence, the above plane-parallel flow field has to be perturbed. To that end, several vortices aligned either with the streamwise x direction or with the spanwise z direction were superposed. Their axes were chosen to lie at $y = 0$, the middle of the channel. The initial flow field thus obtained was guaranteed to be solenoidal. In addition, a random perturbation was imposed on the pressure field, leaving the solenoidal velocity unchanged. Of course, this perturbation propagates immediately in time into all three velocity components, but approximate solenoidality is readily maintained.

The influence of perturbation strength is only qualitative: below certain amplitudes of the vortices turbulence decays; the symmetry–braking effect of random perturbation also competes with viscous diffusion. Too large perturbations are eventually limited by numerical factors. The strength of the streamwise vortices was taken comparable to the mean flow velocity. Spanwise vortices were typically taken twice weaker but of the same radius. Although certain combinations of inclined waves provide the fasted growing modes according to linear stability and have been used successfully in the reference pseudo-spectral DNS [18], neither such waves nor corresponding inclined vortices of higher amplitude and smaller cross-section have been used, thus avoiding the expensive work for their numerical preparation. No "wall roughness" or other flow obstruction has been employed, either.

3.3. DNS methods: pseudo-spectral vs. lattice Boltzmann

The standard for simulating fully developed channel turbulence [18] is a pseudo-spectral method using Chebyshev polynomials in the wall-normal direction and standard Fourier series in the remaining two homogeneous directions. Compared with other methods, spectral and pseudo-spectral methods have maximum accuracy for a fixed number N of degrees of grid points in a given coordinate direction. This is true for both amplitude and phase, for all smooth fields, including multiple derivatives of the basic hydrodynamic fields in a resolved Navier–Stokes DNS, i.e., under the condition that the computational grid is sufficiently refined so that the viscous-scale structures in the flow are resolved. The computational cost of pseudo-spectral algorithms is dominated by that of fast Fourier transforms (FFT). In d-dimensional space, the latter have a cost of order $O(N^d \ln N)$, where N is a representative value for the number of grid points along each of the different coordinate directions.

Multi-dimensional FFTs are implemented as tensor products of one-dimensional (1D) FFT. Using Chebyshev polynomials in the y direction relies on a cosine transform and hence again on an FFT. The 1D FFT transform is non-local—it requires simultaneous processing of all its data. This makes multi-dimensional FFTs also non-local and enforces the need for global communication across computational nodes on a parallel machine in all spatial directions along which the computational domain is split among these nodes. Furthermore, the tensorial nature of such FFTs prevents a strictly local refinement of resolution: in order to improve resolution at the channel centerline, one is forced improve by the same factor the resolution at the wall, but there it is much finer anyway, if Chebyshev discretization is used. In the homogeneous $= sx$ and z directions, the same resolution must be used at all distances from the wall, which means in practice that either too much resolution is carried along in the simulation at points near the centerline, or that the resolution very close to the wall is too low.

Lattice Boltzmann schemes are free from these deficiencies of pseudo-spectral methods. They allow flexible and strictly local grid refinement, but this feature was not used in the present simulations. At higher Reynolds numbers, refinement near the walls would become inevitable, as with any other DNS or LES solver. On the other hand, full advantage was taken of another feature of lattice Boltzmann methods, namely the strictly local and modest communication demand.

The number of operations per time step in lattice Boltzmann codes scales linearly with the grid size. In three-dimensional simulations this means $O(N^3)$ operations, to be compared with $O(Ns^3 \ln N)$ for pseudo-spectral codes. The non-locality of FFT operations means that, no matter how the work along distributed coordinate directions is divided among processors, a data amount needs to be communicated across nodes, which is no less in order than the amount exchanged in an index transposition of the full three-dimensional data array. Hence the communication cost per time step, which is due to d-dimensional FFTs, is $O(N^d)$. Lattice Boltzmann algorithms, on the other hand, need to communicate per time step only the information on the boundaries of the subdomains corresponding to individual computational nodes and the communication is

local, only with the immediate neighbor on the topological processor grid. This reduces the global communication to $O(N^{d-1})$, a dramatic improvement against pseudo-spectral algorithms.

Assuming that the number of processors is fixed, the communication cost per time step in a 3D simulation is $O(N^3)$ for pseudo-spectral and $O(N^2)$ for lattice Boltzmann codes. If the number of processors scales with the linear dimension N of the computational grid—as in the case of very highly parallel architectures consisting of relatively small independent processors whose workload cannot be increased much—the cost of a LB code would scale as $O(N^3)$, whereas FFTs would be too overwhelmed by communications to be considered a practical option.

Like all other explicit methods, lattice Boltzmann methods use smaller time steps when spatial resolution is increased. In turbulence DNS, inertial forces are dominant, so that effectively $\Delta t = O(\Delta)$ must be followed, as opposed to low-*Re* calculations, in which explicit methods must follow $\Delta t = O(\Delta^2)$ and are therefore considered too expensive and replaced by implicit methods. For a fixed physical unit of time, such as t_c, in a turbulence DNS a lattice Boltzmann code would thus require $O(N^3)$ time steps.

This statement also takes into account that the CFL number is comparable in simulations with both types of methods. The experience of the present authors' and other groups with pseudo-spectral direct numerical simulation of turbulence is that a CFL number of 0.4–0.5 can be considered generally safe and can be driven perhaps up to 1, depending on the problem and the code. Experience with lattice Boltzmann simulations and theoretical work suggest that velocities should not exceed a certain v_{max}, which is estimated depending on the precision requirements to be between 0.15 and 0.25 in lattice units. This indicates the range of safe CFL numbers (only twice below those of standard explicit methods) as well as of maximally admissible (numerical) Mach numbers, $0.26 \leqslant v_{max}/c_s \leqslant 0.42$, for the presented direct numerical simulation.

For a fixed number of computational nodes, the communication cost per physical time unit can be evaluated as $O(N^3)$ for LB codes, since $\Delta t = O(\Delta)$, and as $O(N^4)$ for pseudo-spectral codes. The corresponding overall computational cost per physical time unit would then be $O(N^4)$ for lattice Boltzmann codes vs. $O(N^4 \ln N)$ for pseudo-spectral codes. It must be kept in mind, however, that incorporating adaptive time stepping and implicit handling of viscous terms in the latter may influence considerably in its favor the numerical prefactors which are not accounted in the asymptotic estimates given here. Thus, the actual computational requirements of the two types of codes would depend on grid size and code implementation. Based on practical observations, they can be expected to be comparable at the currently practicable $N = O(10^2)$–$O(10^3)$.

In summary, the above asymptotic estimates suggest that lattice Boltzmann codes are overall more efficient than pseudo-spectral codes at least for very large grids. From a practical point of view, it remains to be verified (a) whether the predicted difference in speed is observed already at practically relevant N sizes and (b) whether this does not lead to an unacceptable deterioration of the numerical solution quality. In Sections 4 and 5, respectively, it is shown that in both respects the developed lattice Boltzmann code presents a viable alternative to a Chebyshev pseudo-spectral code for turbulence DNS, even when only the simple geometry of plane channel flow is considered.

3.4. Required resolution for DNS of channel turbulence

In the present context, resolution is characterized by two measures: (i) the overall dimensions of the computational box limit the resolved wavelengths from above and (ii) the uniform step size along the computational grid lines limits the resolved wavelengths from below. It has been documented in the literature on turbulence DNS that the (local) grid step size should not exceed a (local) maximal size Δ_{max} proportional to the (local) dissipative length scale (also called Kolmogorov scale): above $\Delta_{max} = 1.5\eta - 2\eta$ explicit simulations become unstable and implicit or otherwise stabilized computations become incorrect in all aspects influenced in some way by dissipation or by small-scale dynamics in general. A fully resolved simulation is expected to have $\Delta_{max} \leqslant \eta$ and efficiency requires that an approximate equality is maintained in the regions of strongest gradients. In the present lattice Boltzmann simulation, a single uniform grid is used, so $\Delta = \Delta_{max}$.

For fully developed channel turbulence, it can be estimated [23, exercise 7.8] that $\eta^+ \approx 1.5$ at the wall and that η increases with increasing distance from the wall. Hence a uniform grid step size $\Delta^+ \approx 1.5$ would guarantee a fully resolved simulation and $\Delta^+ \leqslant 2.5$ can be expected to give the stability threshold. In practice, it was found in various geometries that $\Delta^+ \leqslant 2.3$ guarantees stability whereas higher values often cause blow-up, but that for some channel flow simulations in particular (cf. the next section) even $\Delta^+ \approx 2.8$ can be useful. The main results, as reported in Section 5, are obtained from a simulation with $\Delta^+ < 1.5$ and indeed found to agree very well with other resolved experiments.

Assuming that the computational domain length in the two homogeneous directions x and z is comparable to the corresponding turbulence correlation lengths, the time required for the accumulation of statistics, when measured in a physical unit such as t_c, is proportional to the time required by the flow to "advect the turbulence" through the whole domain. The main interest here is, as already explained above in relation to the moderate value of the simulated Reynolds number, focused on turbulence statistics in the layers closest to the wall. Therefore, even the slowest advection, which takes place in the viscous sublayer with velocities close to u_τ, had to be taken into account, implying a minimal duration equal to the "flow-through time" $t_f = t_c \alpha_x = 16 t_c$. In the buffer layer and beyond, velocities are in the range 10–$20 u_\tau$ when $Re_\tau = O(10^2)$. However, near the centerline turbulence is rather weak,

implying a turbulent mixing rate that is, for the given Reynolds number, about one order of magnitude lower at the center than at the point of maximum turbulent intensity $y^+ \approx 15$ in the buffer layer. Accordingly, the time of averaging required near the centerline is an order of magnitude longer than that at $y^+ \approx 15$, where it must be at least $10t_c\alpha_x$ since $U^+(15) \approx 11$. Thus, for the Reynolds number considered, the lower limits on the duration of time averaging imposed by the dynamics very close to the wall and by that near to the centerline are close. The estimates they yield were found to agree with the typical duration (depending on initial conditions, on flow domain size in physical time units, on Re_τ, and on the criterion chosen to indicate the statistically steady state) of 10–30t_c of the initial transient in the simulations.

For significantly larger Re, the lower limit (in t_c units) relevant for the turbulence near the centerline would increase and, at the same time, the streamwise correlation length relevant there and thus the computational domain length in x would grow (at least linearly with Re_τ, according to the separate work by the present authors on correlation lengths, already mentioned earlier). Since $Re_\tau = H^+$ implies also a linear growth in the y-length, the overall computational costs would increase faster than $O(Re_\tau^4)$, assuming a single grid and no refinement at the wall.

The arguments above, concerning CFL numbers, reflect the requirement that the flow velocity be uniformly small compared with the "sound speed" as a prerequisite for the lattice Boltzmann scheme to approximate the incompressible Navier–Stokes dynamics. The relative error due to numerical compressibility is $O(v_{max}^2)$. To keep that error below 1%, it is necessary to maintain $v_{max} \leqslant 0.1$ in lattice units. Taking the above crude estimate $20u_\tau$ for centerline velocity as v_{max}, one arrives at $u_\tau = 0.005$ as a precision requirement specific to the flow and the method considered.

Then $t_c = H/u_\tau \geqslant 100N_y$ in lattice units. The well-resolved DNS reported in Section 5 has $N_y = 128$ and an a posteriori value of u_τ close to the above estimate, so that its $t_c \approx 12500$ time steps and its flow-through time $t_f \approx 2 \times 10^5$ steps. Averaging times about one t_f unit were found to suffice for obtaining mean flow profiles, and additional 3–5t_f for the Reynolds stresses, and up to 10t_f for skewness and flatness. Any higher-order statistics take even longer times (in t_c units) to converge.

4. Implementation and performance

A parallel solver implementing the lattice BGK method for some of the popular lattice models has been developed for the purpose of turbulence DNS and LES, and accordingly named "Boltzmann Equation Solver Tool" (BEST). The implemented models are D2Q9 for two-dimensional and D3Q15, D3Q19, and D3Q27 for three-dimensional computations. For each of these models, the corresponding "incompressible" version is implemented, including the D3Q19i model described in Section 2.2 and used throughout for the simulations reported in this paper. For some of these lattice models, corresponding multiple-relaxation-time schemes available in the literature have also been implemented.

4.1. Parallelization

BEST has been ported to a broad range of high-performance computer architectures, including the pseudo-vector Hitachi SR8000-F1, the pure vector machines of the Fujitsu VPP and NEC SX series, the massively parallel Cray T3E, and the RICS architectures of SGI Origin and Sun. For shared memory architectures BEST is parallelized using OpenMP and for distributed memory architectures using MPI.

On all platforms that support vectorization, a degree of vectorization over 90% and a corresponding efficiency of over 50% of the peak performance on a single vector processing node have been achieved. For better performance on the Hitachi SR8000-F1, an inner node parallelization technique (COMPAS) developed by Hitachi is used. This assures some 30% of the theoretical peak performance of the machine, corresponding to 21 Mlups on one node. The unit of 1 Mlups $= 2^{20}$ lattice-site updates per second has become a standard measure of performance for lattice Boltzmann applications. The parallel speedup with increasing number of nodes used in a test computation with BEST and the absolute performance in Gflops (1 Gflops $= 2^{30}$ floating-point operations per second) can be seen in Fig. 1.

4.2. BGK vs. MRT models

For the simulations presented in this paper, BEST was run with the BGK D3Q19i model. With a multiple-relaxation-time model, an improvement of the solver's stability and/or a reduction of the number of probabilities f_α advanced in time is possible. In weighing up the factors involved here, a specific aspect of turbulence DNS must be kept in mind: all length scales down to the Kolmogorov scale η need to be resolved. It was already noted in Section 3.4 that the grid step size $\Delta = \Delta^+\delta_\tau$ should not exceed 2η, and that for wall-bounded turbulence this corresponds to $3\delta_\tau$. It was also noted that in practice the BGK D3Q19i model is stable for $\Delta \leqslant 2.3\delta_\tau$. Hence the maximum reduction in grid size achievable by switching to a more stable model would be λ^3, where $\lambda \geqslant 2.3/3$, i.e., the total grid size can be reduced to not less than 45% of the size of the BGK grid.

This observation is not, as may seem at first glance, in contradiction with the impressive demonstration of the stability of multiple-relaxation-time simulations, given in [6] and implying a possible reduction in grid size by a factor of at least 4^d, i.e., down to 15% of the BGK grid in the present case. Indeed, the careful claim made in [6] is that the position and shape of a large-scale structure, whose thickness is difficult to resolve on the coarse grid, is still captured by the MRT version of a scheme based on the D2Q9 lattice (which can be obtained by a 3D-to-2D projection of the

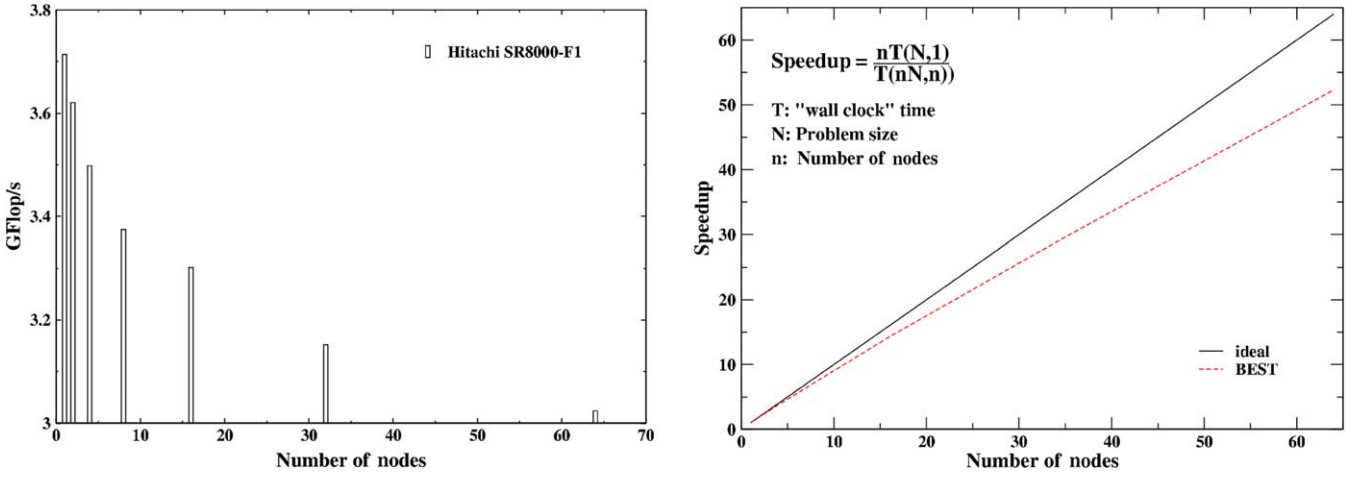

Fig. 1. Speedup of the MPI-parallelized code BEST, in D3Q19 lattice BGK mode, on the pseudovector distributed-memory platform Hitachi SR8000-F1.

D3Q19 lattice used here) whereas the BGK method for the same lattice becomes unstable. The point is that the fine structure, in that case the correct cross-sectional thickness and profile of a thin vorticity layer, is not resolved by the MRT method either, as it does not fit properly on the grid anyway, independent of the method used.

Numerical experiments aimed at quantifying the possible advantages of using MRT schemes in (necessarily three-dimensional) direct numerical simulation of turbulence are under way. The situation for LES and even more for simulations at low Reynolds numbers is, of course, well known to be different: MRT schemes are clearly superior in most of those cases.

4.3. Lattice Boltzmann vs. Chebyshev pseudo-spectral method

A comparison between the asymptotic performance of the lattice Boltzmann and the Chebyshev pseudo-spectral method was given in Section 3.3 and lattice Boltzmann methods were claimed to be superior for large grids. However, it was also pointed out that it is of practical importance to compare the actual costs of the two types of methods at the moderate resolutions and the corresponding moderate Reynolds numbers which are currently achievable by direct numerical simulations and at which the asymptotic scaling with grid size is not yet established. For a fair comparison, the number of grid points was prescribed and the CPU time required to advance a developed channel flow over one physical time unit t_c was measured. This allowed the standard Chebyshev pseudo-spectral code to take advantage of its elaborate adaptive and implicit time-stepping procedure, and also of the optimal FFT package among a number of available options. A nominal Reynolds number of $Re_\tau \approx 180$ and a grid size of 128^3 grid were prescribed.

BEST uses fixed time step and cubic grid cells; its spatial resolution was $\Delta^+ = 2.8$. The Chebyshev pseudo-spectral code was a version of the code with which the standard database [21] was generated. In the direction normal to the wall it uses Chebyshev collocation and correspondingly a non-uniform grid, so its y-step between neighboring grid points varies from $\Delta^+ = 0.16$ between the two points closest to the wall to $\Delta^+ = 4.34$ at the center of the channel. As a result, the lattice Boltzmann grid gives a finer spatial resolution along the y direction than the Chebyshev pseudo-spectral grid at distances $y^+ > 10$ off the wall. With these specifications, it was found that a run on a single node of the Hitachi SR8000-F1 takes 32 min with BEST vs. 158 min with the Chebyshev pseudo-spectral code.

5. Results

The results reported below consist of one-point (meaning also single-time) statistics obtained from time and space averaging (along the parallel walls) during sufficiently long direct numerical simulations. The main purpose of presenting the following statistics is a validation of lattice Boltzmann method as turbulence DNS solvers. It is based on a comparison between pseudo-spectral and lattice Boltzmann DNS data at fixed Reynolds number. To appreciate further the quality of agreement between results obtained by the two different types of numerical methods, their results are compared with laboratory measurement data in several important instances for which suitable experimental measurements have been available to the present authors. Sufficiently resolved DNS should differ visibly only if there are noticeable variations in some of the physical parameters of the run set-ups. Generally, such a difference should be smaller than the scatter of experiments in similar set-ups.

5.1. Specification of the reference simulation

With the grid size and Re_τ value considered at the end of the previous section, the lattice Boltzmann grid resolution is $\Delta^+ \approx 2.8$ near the wall. The results reported below are from a grid with twice as fine resolution: still for $Re_\tau \approx 180$

but with 4192:256:256 grid points and thus a $\Delta^+ = 1.44$. As discussed in Section 3.4, such a Δ^+ value guarantees a reliable, fully resolved DNS. Although meshes stretched in the streamwise direction are, in principle, applicable to lattice Boltzmann simulations and are used as a standard set-up in pseudo-spectral simulations, they are not used here, for two reasons: (i) the methodology is still new in the lattice Boltzmann context and thus not completely tested and optimally documented yet and (ii) having a uniform grid step in all three directions guarantees that nearly isotropic turbulence near the channel center and small-scale perturbations near the wall are properly resolved.

The very large number of grid points in the streamwise direction, 2^{12}, was decided upon on the basis of extended tests on the effect of streamwise and spanwise size, in physical units, of the computational domain. These tests suggest that the "minimal channel" has a length of 4000–6000 in wall units, as far as only low-order one-point statistics and only moderate Reynolds numbers, $Re_\tau = O(10^2)$, are concerned. Higher Reynolds numbers and more complicated statistics require even longer domains to be evaluated reliably, as discussed in Section 3.4. The cost of such direct numerical simulations would reach beyond the purpose and the means of the present investigation.

Concerning pseudo-spectral DNS, a repetition was carried out, as precisely as practically possible, of the reference DNS at $Re_\tau \approx 180$ [21]. This was made with a version of a code (written at NASA and kindly provided for the present purpose by R. Moser) which was used to produce the original database [21]. The differences between the present Chebyshev pseudo-spectral computations (whose detailed description is given in [26]) and that publicly available database can be due to two factors: a difference in the time span of averaging, or a difference in initial conditions. Both of these factors are definitely present and are due to the minor incompletenesses in the specifications that can be extracted from the reference database and by tracing back its references.

Both Chebyshev pseudo-spectral simulations, that of [21] and the in-house one, were driven by enforcing a constant flux, whereas the BEST simulation is forced by a constant pressure drop. The initial flow fields used by the two different codes are also entirely different. The very good agreement between the results extracted from such independent simulations emphasizes the good quality of each of them individually.

5.2. Mean profiles

The computation of a correct mean velocity is the easiest and first necessary test for a turbulence simulation. It is passed successfully by many different numerical methods. BEST is no exception to this rule. As seen in Fig. 2, the comparison with the reference database [21] and also with experimental data [10] is very good. The figure compares profiles not only of (streamwise) mean velocity but also of mean pressure. Normalization is by u_τ and u_τ^2, respectively. For the latter case, it is recalled that $\rho = 1$ both in the present "incompressible" lattice Boltzmann and in the reference pseudo-spectral data.

The good agreement for the mean pressure P is a less obvious result than the agreement for the mean velocity U. By construction, lattice Boltzmann methods are weakly compressible and even the "incompressible" lattice Boltzmann model used here is in essence an artificial compressibility scheme, as discussed in Section 2. This may obviously affect the fluctuating pressure, as seen further below. It is argued, however, that it should not affect the mean pressure distribution, provided that the averaging is performed late and long enough to yield converged Reynolds stresses. The quality of the average pressure profile obtained from the lattice Boltzmann simulation is confirmed in Fig. 3, using the exact relation

$$P(y) + R_{yy}(y) = \text{constant}. \tag{27}$$

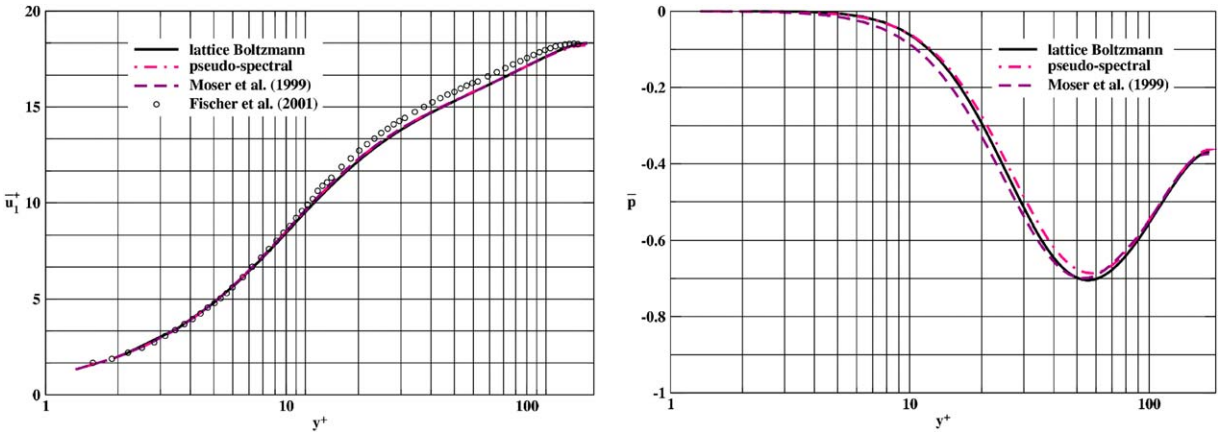

Fig. 2. Comparison of lattice Boltzmann and Chebyshev pseudo-spectral results for *mean profiles*: left, streamwise velocity; right, pressure. Line styles: solid, BEST; dashed, Chebyshev pseudo-spectral data from [21]; dash-dotted, Chebyshev pseudo-spectral data from in-house DNS [26]; symbols, experimental data from in-house LDA measurements [10].

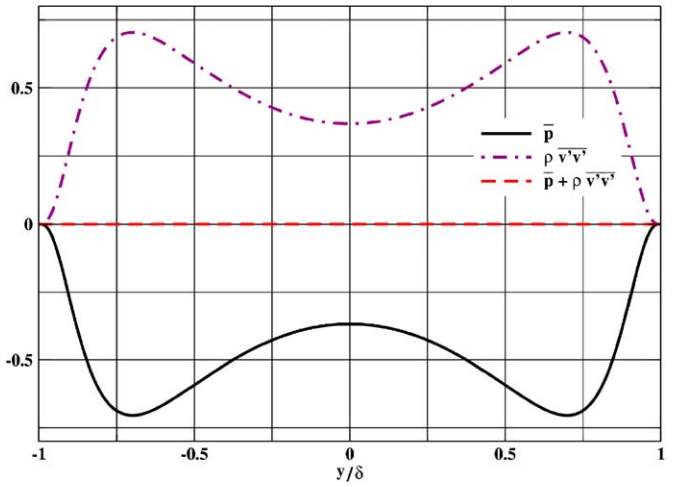

Fig. 3. Confirmation of the analytic relation between mean pressure and wall normal Reynolds stress profiles. Normalization is with ρu_τ^2, as explained in the text.

The agreement of data with the constraint (27) can also be seen indirectly, by comparing the P plot in Fig. 2 and the R_{yy} plot in Fig. 5.

The analytic relation (27) is derived from the y-momentum equation, which is approximated by the D3Q19i model to $O(Ma^3)$ errors (against $O(Ma^2)$ with the standard D3Q19), while pressure fluctuations scale as $O(Ma^2)$. It is therefore expected that (27) will be satisfied by the lattice Boltzmann simulation data to the usual degree of precision, to which the instantaneous simulated fields are accepted to approximate the Navier–Stokes dynamics. The mass conservation equation is given to the same degree of approximation by (21), which cannot be distinguished at that order of precision (and recalling that $\rho = 1$) from the scalar advection equation

$$\partial_t p + \nabla_{\boldsymbol{x}} \cdot (\boldsymbol{v} p) = 0. \tag{28}$$

As indicated in Section 2.4, this equation is exact for the original D3Q19 model, from which the "incompressible" D3Q19i is derived. The same is true for all other lattice models in use. This suggests that compressibility errors may well be $O(Ma^2)$ in regions with fast time variations and strong gradients. Examples of such regions are the fast and strong non-linear waves determining the intermittent turbulence structure close to a flat wall, and regions of hyperbolic large-scale flow, where small-scale vorticity is generated and turbulent energy cascaded to shorter scales. The latter kind of regions are also known to exhibit the strongest gradients of advected scalar fields. It may therefore be expected that at least during transient evolution, the turbulent pressure field predicted by lattice Boltzmann simulations will resemble in regions of the described kind the structure of a passive scalar field.

A qualitative illustration of such resemblance is provided in Fig. 4. At early times of flow development, large-scale spanwise vortex structures inherited from the initial condition can be recognized, as seen on the first plot in the form of large, empty regions (visualizing with a different threshold for p or using vorticity instead of p shows them more clearly). These structures stretch and thin out the vorticity, but also any advected scalar field, in the narrow spaces between them. These regions are clearly seen on the same plot. At later times in the evolution, when the near-wall flow structure maintaining the statistically steady-state channel turbulence has more or less been set up, there are no fast transients in the large-scale structure and the extremities of pressure fluctuation are localized near the wall, where the strongest vortices are found in close spatial correlation with low-speed streaks. The corresponding different kind of distribution of pressure extremes is well recognizable on the second plot in the same figure. Localization of pressure minima inside vortices is an expected, correct behavior.

5.3. Reynolds stresses

The presented simulation provides predictions for the y-distributions of individual Reynolds stress components. Lattice Boltzmann and pseudo-spectral results are shown in Fig. 5 normalized by the "wall units" u_τ and δ_τ. For the diagonal stress components, the componental r.m.s. turbulent energy is shown instead of the Reynolds stress itself, accordingly denoted by $u_{\mathrm{rms}} = R_{xx}^{1/2}$, $v_{\mathrm{rms}} = R_{yy}^{1/2}$, $w_{\mathrm{rms}} = R_{zz}^{1/2}$. The overall quantitative agreement is very good. Some available experimental data have been added in that figure to illustrate the expected smallness of the difference between numerical results compared with the deviation of experimental data. Deviations between lattice Boltzmann and Chebyshev pseudo-spectral results are noticeable only for the streamwise velocity component u,

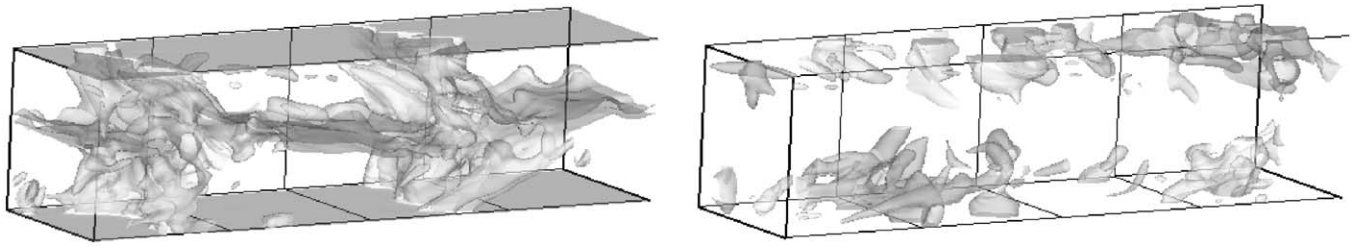

Fig. 4. Isosurfaces of pressure computed by the "incompressible" D3Q19i model. The snapshots shown were taken at the following approximate times from flow initialization: $7.5t_c$ (left) and $12t_c$ (right). The time unit t_c is discussed in Sections 3.1 and 3.4.

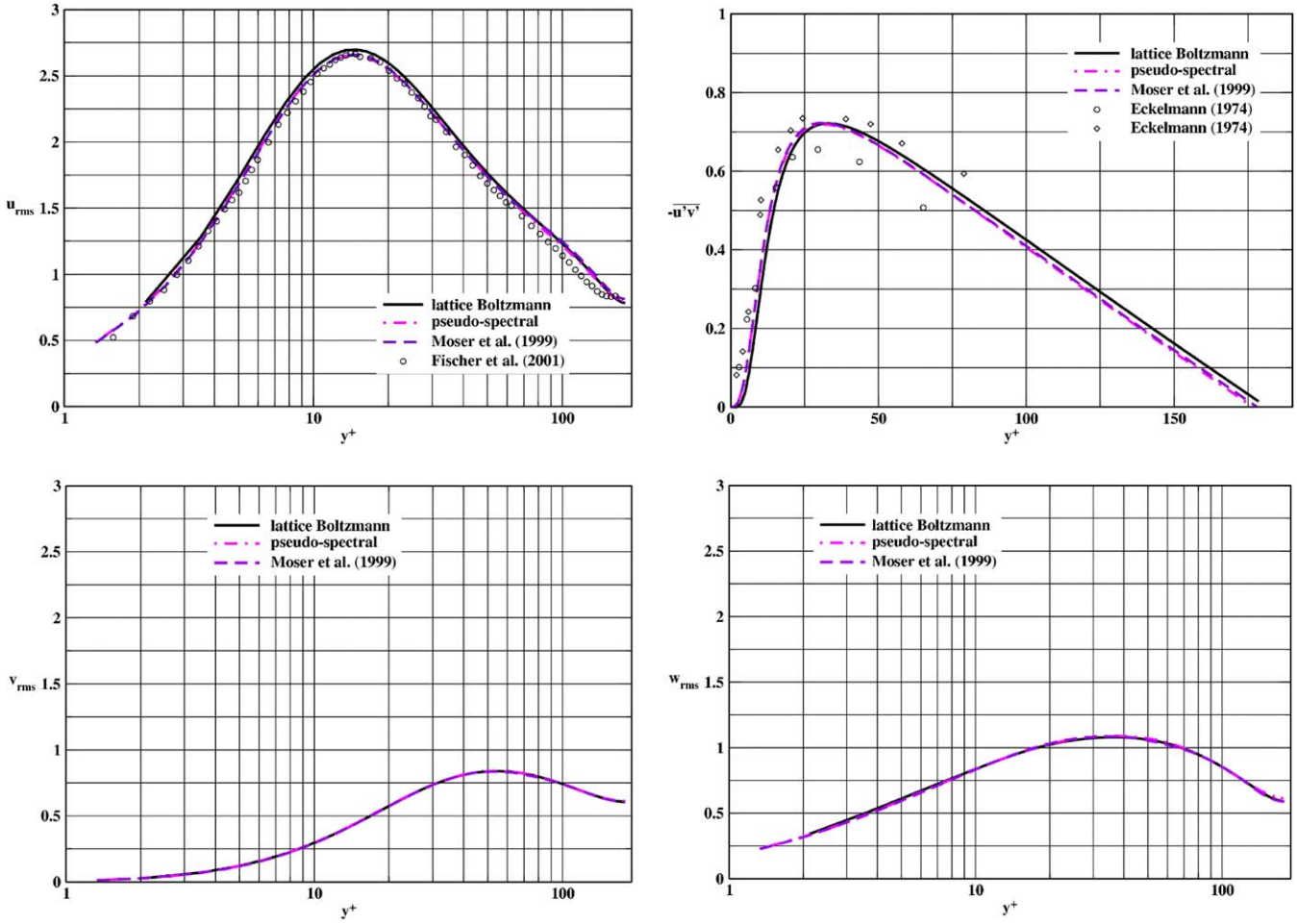

Fig. 5. Comparison of lattice Boltzmann and Chebyshev pseudo-spectral results for the second moments of fluctuating velocity: upper left, streamwise velocity intensity; upper right, Reynolds stress; lower left, wall-normal velocity intensity; lower right, spanwise velocity intensity. Line styles as in Fig. 2.

but remain small. The maximal discrepancy is near the peak of u and can be attributed to differences in the flow domain length and the number and time span (in physical units) of sampled velocity fields, rather than to essential differences in the effectively simulated dynamics.

The most significant discrepancies between the two methods can be observed for the moments of fluctuating pressure. The treatment of pressure in lattice Boltzmann schemes is fundamentally different from that in pseudo-spectral methods.

At the level of second moments, which is presented in this section, the pressure analog of componental turbulent velocity intensities shown above is $p_{\mathrm{rms}} = \langle (p')^2 \rangle^{1/2}$. The corresponding estimates from lattice Boltzmann and Chebyshev pseudo-spectral DNS are shown in Fig. 6, normalized by ρu_τ^2. The lattice Boltzmann data predict a somewhat higher intensity, which can be interpreted as the effect of a loss of precision in comparison with pseudo-spectral data. The nearly constant and relatively small difference between the two types of data confirms this interpretation. It may be noted in this respect, that the cause of spurious pressure fluctuations in lattice Boltzmann simulations is well understood [7] and that the lattice BGK is unfavorable in this respect.

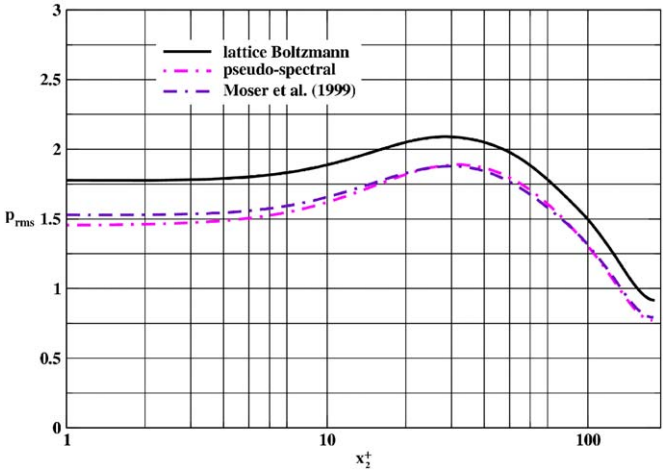

Fig. 6. Comparison of lattice Boltzmann and Chebyshev pseudo-spectral results for the r.m.s. values of the pressure fluctuations. Line styles as in Fig. 2.

5.4. Skewness and flatness factors

The most stringent test presented here is a comparison of higher-order one-point statistics, namely y-distributions of the skewness and flatness of fluctuating pressure and individual components of fluctuating velocity. The skewness and flatness profiles for the spanwise velocity are shown in Fig. 7. It can be seen that differences between the BEST results and the reference DNS database are unsystematic and small for S_3 (the large deviation near the centerline in the data from [21] is apparently due to insufficient domain length or sample number, affecting the averages in [21]) and are surprisingly small for F_3, being comparable to the differences between two runs with essentially the same Chebyshev pseudo-spectral code. Having in mind the differences in the numerical approximation, the domain size, the forcing and initial conditions, this presents strong evidence for the reliability of all three simulations considered.

The skewness profiles $S_1 = S[v'_x]$ and $S_2 = S[v'_y]$ of the streamwise and wall-normal turbulent velocity components are presented in Fig. 8. The comment of the S_2 results is essentially the same as for S_3, with the additional note that this time the profile is non-trivial, so the good agreement is quantitatively clear. As for the S_1 profile, for which high-quality in-house experimental data were available [5], excellent agreement between laboratory and numerical experiments is obtained if for each different distance from the wall the better resolved numerical data over that region are taken. It is recalled that the lattice Boltzmann grid was finer at $y^+ > 10$, whereas near the wall the Chebyshev pseudo-spectral code has a finer grid and is expected, also on the theoretical ground of having a superior nominal precision, to yield higher effective precision. In the region near the centerline, the sensitivity to domain length and averaging duration is demonstrated again, as in the case of S_3.

Corresponding flatness profiles $F_1 = F[v'_x]$ and $F_2 = F[v'_y]$ are given in Fig. 9. The comment on F_1 is essentially

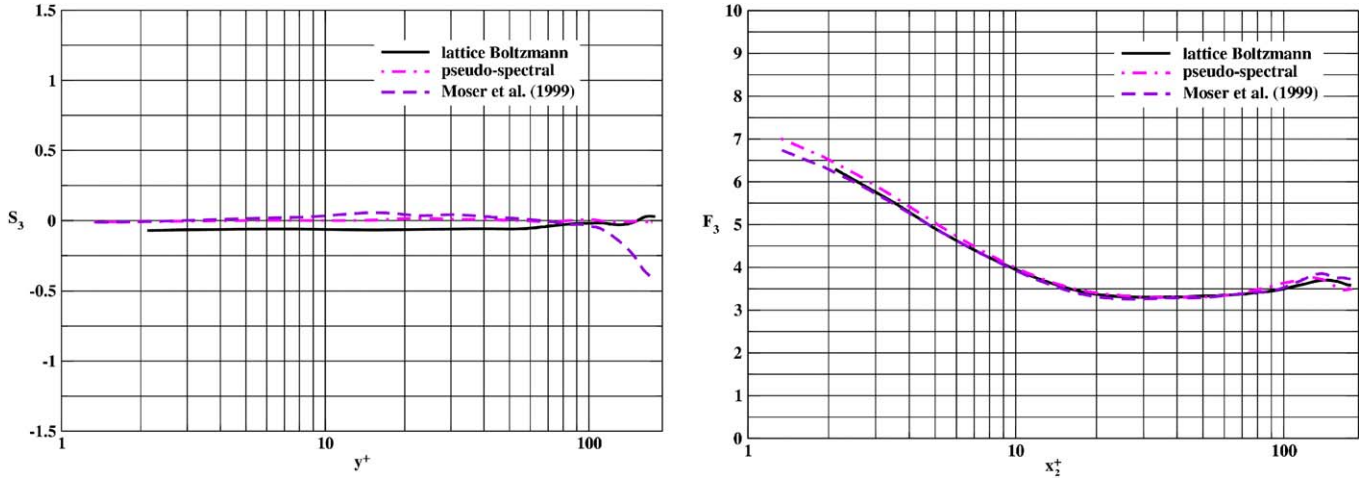

Fig. 7. Normalized higher-order moments of spanwise velocity: left, skewness; right, flatness. Line styles as in Fig. 2.

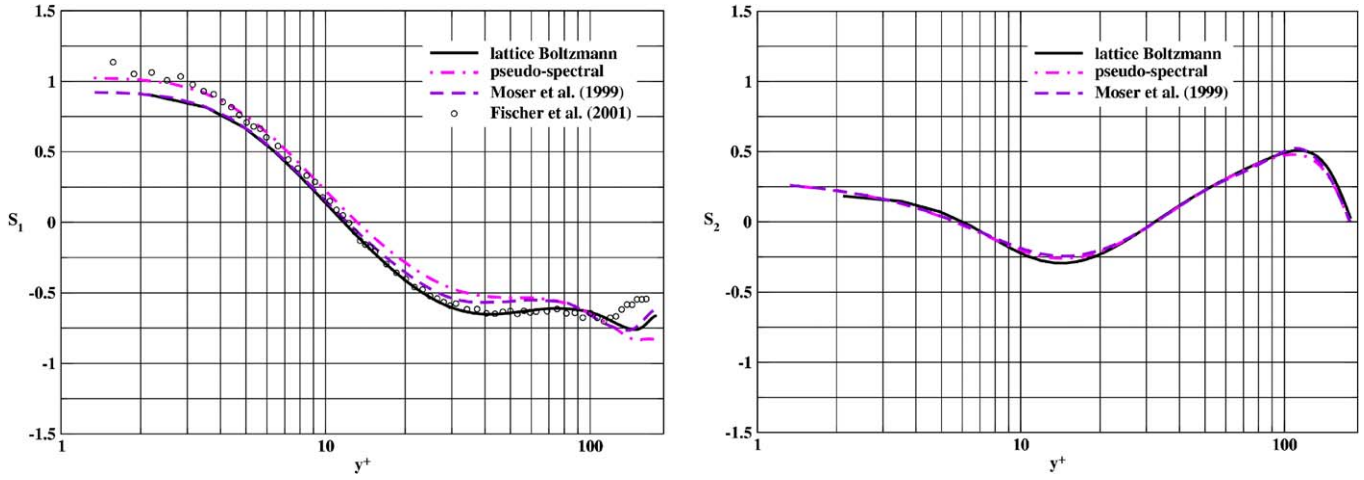

Fig. 8. Comparison of lattice Boltzmann and Chebyshev pseudo-spectral results for the *skewness* of velocity components: left, streamwise velocity; right, wall-normal velocity. Line styles as in Fig. 2.

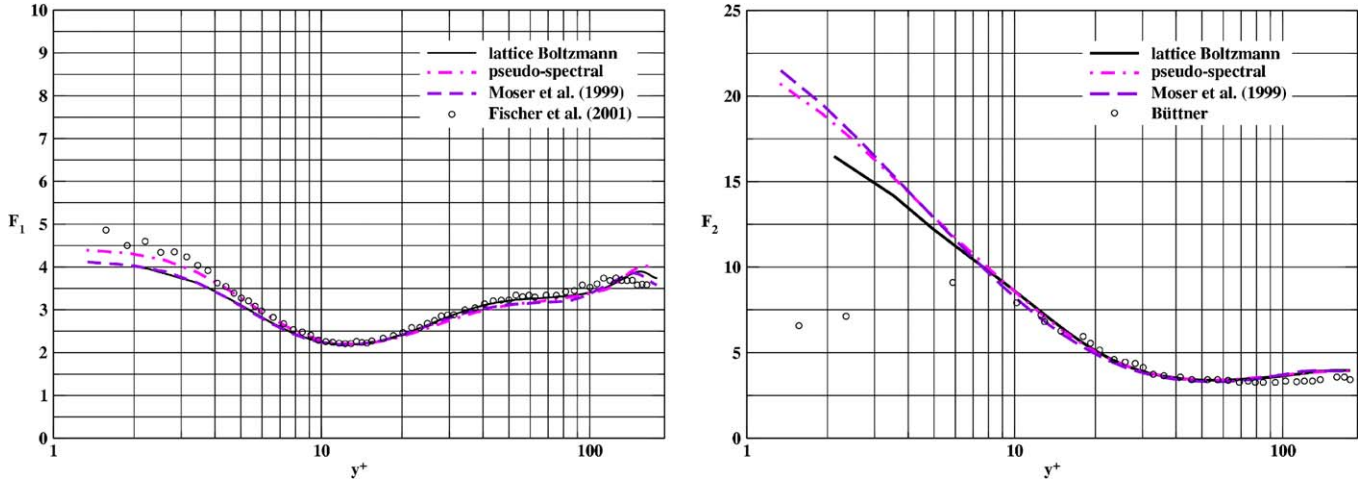

Fig. 9. Comparison of lattice Boltzmann and Chebyshev pseudo-spectral results for the *flatness* of velocity components: left, streamwise velocity; right, wall-normal velocity. Line styles as in Fig. 2. Symbols show experimental data from in-house LDA measurements [5].

the same as for S_1, with the additional note that in the viscous sublayer, which occupies the region closest to the wall, say $y^+ < 7$, the discrepancies become unusually large compared with the rest of the flow domain. Moreover, the disagreement between the two Chebyshev pseudo-spectral simulations is comparable to that between the different simulation methods and laser-Doppler anemometry (LDA) laboratory measurements. This suggest the presence of a numerical problem, which is corroborated by the even larger discrepancies observed also in F_2 over precisely the same y^+-extent. The very high F_2 values obtained from pseudo-spectral DNS have triggered an ongoing discussion in the turbulence research community, concerning their physical plausibility and meaning. The trend of increasing $F_2(y^+)$ with decreasing y^+, i.e., as the wall is approached, is also observed in the lattice Boltzmann data, but the latter are seen to predict relatively lower values. The F_2 data represent the only case in which a clear difference between the two numerical methods can be seen.

Reliable experimental measurements of flatness factors, especially for the v_y velocity component, which becomes vanishingly small near the wall not only in absolute value but also in comparison with the other two velocity components, is certainly difficult. It has nevertheless been possible to set up a robust and precise processing procedure for LDA measurements of v_y, which allows the estimation of $F_2(y)$ for distances y well inside the viscous sublayer. Such flatness data obtained from in-house LDA measurements are also shown in Fig. 9. Their clear implication is to corroborate the suspicion about an inaccurate representation by direct numerical simulations of the fine velocity structure near the wall. It has become an article of faith that Chebyshev pseudo-spectral DNS are very precise, especially near the wall. However, the present results cast doubt on its universal validity, in particular for higher-order, normalized statistics, that are generally known to be difficult to measure. In an analytic investigation a fundamental source of errors that contaminate normalized velocity statistics and can, in particular, entirely corrupt the statistics of v_y has been identified: a weak singularity of the normalized velocities v_x/y, v_y/y^2, and v_z/y is mathematically possible and, unless any specific physical mechanisms that prevent it are not properly accounted for, is indeed present in the numerical solution (see [8]). This explains the discrepancies, localized to the viscous sublayer, observed in the predictions of all three velocity flatness factor profiles, and also their much larger amplitude in the case of F_2. The same theoretical considerations have also provided a simple interpretation of the seemingly paradoxical observation that the nominally more precise Chebyshev pseudo-spectral method suffers larger deviations of its F_2 predictions, as compared with the lattice Boltzmann method.

Finally, the fluctuating pressure skewness and flatness distributions are presented. As can be seen in Fig. 10, the discrepancies and fluctuations in the predictions obtained from the two Chebyshev pseudo-spectral DNS are so large, that over most of the flow domain they cannot be considered reliable. The profile trends which the in-house Chebyshev pseudo-spectral DNS data exhibit are nevertheless in qualitative agreement with the lattice Boltzmann data and can be considered plausible: the pressure skewness vanishes at the wall and tends to 0.5 near the centerline, a value that is in expected agreement with skewness data for isotropic turbulence. The flatness is constant in the viscous sublayer and exhibits a moderate increase towards the centerline. A systematic difference in lattice Boltzmann data from pseudo-spectral data is found for S_p beyond the viscous sublayer and for F_p over the whole flow domain. Over the viscous sublayer, the lattice Boltzmann predictions for both statistics essentially coincide with their values for Gaussian noise. Physically, large-scale pressure fluctuations are weak over the width of that narrow layer and strong but well localized, intermittent structures determine the flow statistics. The presence of broadband noise would influence the signal from such structures much more than that from large-scale ones. Therefore, the

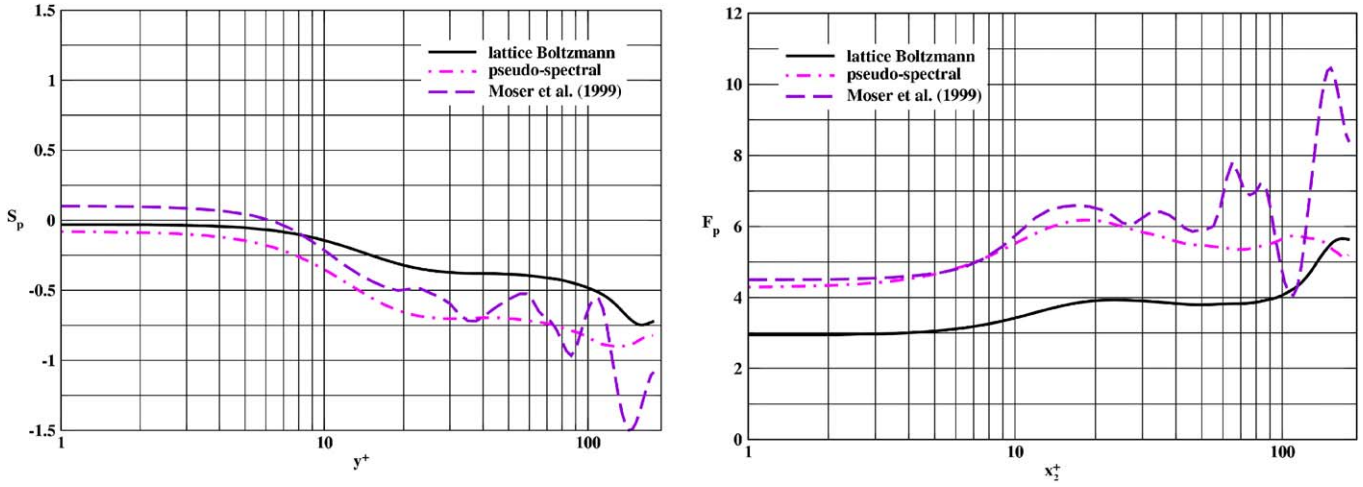

Fig. 10. Normalized higher-order moments of pressure: left, skewness; right, flatness. Line styles as in Fig. 2.

closeness of the lattice Boltzmann data for skewness and flatness to the respective Gaussian values can be interpreted as yet another piece of indirect evidence for the noisiness of fluctuating pressure, whose origin was discussed in the preceding sections.

6. Conclusion

The class of lattice Boltzmann methods which has been developed very intensively over the last decade is shown in this study to provide a robust, highly efficient and adequately precise approach to the direct numerical simulation of incompressible turbulence. Lattice Boltzmann algorithms are simple, fast, and perfectly suited for the vector and parallel execution paradigms of high-performance computing in its present state. In order to show that lattice Boltzmann codes offer an excellent compromise between the requirements for speed and precision, it remains to be verified that they produce reliable turbulence statistics in various types of turbulent flows. Attempts to validate and use lattice Boltzmann schemes for direct numerical simulation of 3D turbulence have remained limited, with little progress reported recently. Tests have focused on homogeneous isotropic turbulence and on developed channel flow turbulence, with a couple of publications in each case. The numerical effort in all of these earlier tests has been too limited to allow reliable comparisons with standard data. Meanwhile, an increasing number of engineers are using lattice Boltzmann methods for DNS and LES of turbulent shear flows, with confidence but without thorough verification.

Here, a high-resolution DNS of plane-channel turbulence at $Re_\tau = 180$ has been reported, using a lattice Boltzmann method based on a BGK (single relaxation time) model. The quality of the simulation was evaluated by comparing one-point turbulence statistics obtained from it with two data sets from direct numerical simulations by a Chebyshev pseudo-spectral method and further by appreciating the significance of the observed differences with respect to their deviation from high-quality LDA laboratory measurement data.

The results demonstrate that even the simplest lattice Boltzmann method produces statistics of the same quality as pseudo-spectral methods, at resolutions comparable to, and in fact overall better than, those of the Chebyshev pseudo-spectral runs. It achieves this at a competitive computational cost. In experiments reported only briefly in Section 4, the resolution was reduced by a factor of two in each dimension, compared with the direct numerical simulation reported in detail in Section 5, in order to explore the stability and resolution limits of the method. Computed statistics remained good.

It was shown that some of the higher-order statistics are very sensitive, at least over part of the flow domain, and that neither the pseudo-spectral nor the lattice Boltzmann method can be considered a reliable means to evaluate them at such locations. Correspondence with other groups has confirmed similar problems with all other customary methods for turbulence DNS. In particular, the anomalous high flatness of the normal velocity measured close to the wall from DNS data appears to be plagued by a serious numerical imprecision, the mechanism of which has been investigated in [8].

The lattice Boltzmann data on velocity statistics lie either between the Chebyshev pseudo-spectral and the experimental data or between the two sets of pseudo-spectral data. This removes any doubt that lattice Boltzmann methods have inferior resolution and performance in resolved DNS. Such doubts originate from the second-order convergence of lattice Boltzmann methods with refinement of grid resolution vs. the "exponential" convergence of pseudo-spectral methods (which is, of course, only assured at high enough resolution) and in addition from the Chapman–Enskog expansion, which underlies any lattice Boltzmann method and which assumes some excess of resolution. In particular, the high resolutions required in turbulence DNS make the first-order precision of the "bounce-back" rule at smooth channel walls an issue of

negligible practical relevance. In the case presented here, bounce-back is of second order. Another concern, namely that the quasi-compressible nature of lattice Boltzmann methods would produce imprecise mean pressure statistics, has also been alleviated.

The results presented show that, as far as turbulence statistics are concerned, lattice Boltzmann codes are as reliable as Chebyshev pseudo-spectral codes. Moreover, lattice Boltzmann methods have comparable or lower computational cost. The simplicity and robustness of lattice Boltzmann codes and the optimal scaling of their computational time with increasing problem size are well known and have not been discussed here. These features, together with the results summarized above and the high-performance computing efficiency which was demonstrated for the BEST code implementation presented in Section 4, suggest that lattice Boltzmann methods and in particular the simple and efficient single-relaxation-time lattice BGK algorithm are potent candidates for turbulence DNS and LES in the large-scale, high-Reynolds-number, complex geometry problems that still await a numerical attack. At the same time, it must be kept in mind that, although robust in general, lattice Boltzmann methods cannot avoid the physically determined instabilities and imprecisions encountered by the other numerical schemes.

Acknowledgements

The work presented was funded by KONWIHR, through the BESTWIHR project and through grant DU101/58-1 from the Deutsche Forschungsgemeinschaft. The authors are very grateful for this support. The production runs were carried out on Hitachi SR8000-F1 and VPP700 machines in the Leibnitz Computing Center (LRZ) at the Technical University Munich. The support of the Regional Computing Center (RRZE) at the University of Erlangen–Nuremberg, the John von Neumann Institute for Computing (NIC) in Jülich and the Computing Center at the University of Bayreuth is gratefully acknowledged.

References

[1] Amati G, Succi S, Piva R. Massively parallel lattice-Boltzmann simulation of turbulent channel flow. Int J Mod Phys C 1997;8(4):869–78.

[2] Benzi R, Succi S, Vergassola M. The lattice Boltzmann equation: theory and applications. Phys Rep (Rev Sect Phys Lett) 1992;222(3):145–97.

[3] Bhatnagar P, Gross EP, Krook MK. A model for collision processes in gases. I. Small amplitude processes in charged and neutral one-component systems. Phys Rev 1954;94(3):511–25.

[4] Buick J, Greated C. Gravity in lattice Boltzmann model. Phys Rev E 2000;61(6):5307–20.

[5] Büttner R. LDA measurements in the near-wall region of an axisymmetric sudden expansion. Diploma work, University of Stuttgart and University of Erlangen–Nuremberg, 1995.

[6] Dellar PJ. Incompressible limits of lattice Boltzmann equations using multiple relaxation times. J Comput Phys 2003;190:351–70.

[7] d'Humières D, Ginzburg I, Krafczyk M, Lallemand P, Luo L-S. Multiple-relaxation-time lattice Boltzmann models in three dimensions. Phil Trans Roy Soc Lond A 2002;360(1792):437–52.

[8] Durst F, Beronov KN. On the difficulties in resolving the viscous sublayer in wall-bounded turbulence. In: Friedrich R, Geutrs B, Métais O, editors. Direct and large-eddy simulation V: Proceedings of the 5th ERCOFTAC workshop on LES, September 27–30, 2003. Munich, Berlin: Springer; 2004. p. 43–58;
Beronov KN, Durst F. Mathematical singularity and physical intermittency of the incompressible viscous sublayer. In: Andersson HI, Krogstad PÅ, editors. Advances in turbulence X: Proceedings of the 10th European turbulence conference, CIMNE (publication of the International Center for Numerical Methods in Engineering), Barcelona. 2004. p. 615–8.

[9] Eggels JGM. Direct and large-eddy simulation of turbulent fluid flow using the lattice-Boltzmann scheme. Int J Heat Mass Transfer 1996;17:307–23.

[10] Fischer M, Jovanović J, Durst F. Reynolds number effects in the near-wall region of turbulent channel flows. Phys Fluids 2001;13:1755–67.

[11] Guo Z, Shi B, Zheng C. A coupled lattice BGK model for the Boussinesq equations. Int J Num Meth Fluids 2002;39:325–37.

[12] He X, Luo L-S. Lattice Boltzmann model for the incompressible Navier–Stokes equation. J Stat Phys 1997;88(3/4):927–44.

[13] He X, Luo L-S. A priori derivation of the lattice Boltzmann equation. Phys Rev E 1997;55(6):R6333–6.

[14] He X, Luo L-S. Theory of the lattice Boltzmann method: from the Boltzmann equation to the lattice Boltzmann equation. Phys Rev E 1997;56(6):6811–7.

[15] He X, Zou Q, Luo L-S, Dembo M. Analytic solutions of simple flows and analysis of nonslip boundary conditions for the lattice Boltzmann BGK model. J Stat Phys 1997;87(1/2):115–36.

[16] Jiménez J, del Álamo JC, Flores O. The large-scale dynamics of near wall turbulence. J Fluid Mech 2004;505:179–99.

[17] Jiménez J, Pinelli A. The autonomous cycle of near wall turbulence. J Fluid Mech 1999;389:335–59.

[18] Kim J, Moin P, Moser R. Turbulence statistics in fully developed channel flow at low Reynolds number. J Fluid Mech 1987;177:133–66.

[19] Kim K, Adrian RJ. Very large-scale motion in the outer layer. Phys Fluids 1999;11(2):417–22.

[20] Krafczyk M, Tölke J, Luo L-S. Les based on multiple relaxation time lb model. Int J Mod Phys B 2003;17(1–2):33–9.

[21] Moser R, Kim J, Mansour N. Direct numerical simulation of turbulent channel flow up to $Re_\tau = 590$. Phys Fluids 1999;11(4):943–5.

[22] Perry AE, Chong MS. On the mechanism of wall turbulence. J Fluid Mech 1982;119:173–217.

[23] Pope SB. Turbulent flows. Cambridge: Cambridge University Press; 2000.

[24] Qian YH, d'Humières D, Lallemand P. Lattice BGK models for the Navier–Stokes equation. Europhys Lett 1992;17(6):479–84.

[25] Toschi F, Amati G, Succi S, Benzi R, Piva R. Intermittency and structure functions in channel flow turbulence. Phys Rev Lett 1999;82(25):5044–7.

[26] Volkert R, Breuer M, Durst F. Enhanced direct numerical simulations of the plane channel flow based on a spectral method. Technical report. Lehrstuhl für Strömungsmechanik, Universität Erlangen—Nürnberg, 2002.

[27] Yang ZL, Palm B, Sehgal BR. Numerical simulation of bubbly two-phase flow in a narrow channel. Int J Heat Mass Transfer 2002;45:631–9.